DOI https: //doi. org/10.1007/s11595-024-2864-z

Improvement of Microstructure and Mechanical Properties of Rapid Cooling Friction Stir-welded A1050 Pure Aluminum

XU Nan, LIU Lutao, SONG Qining, ZHAO Jianhua, BAO Yefeng
(College of Materials Science and Engineering, Hohai University, Changzhou 213200, China)

Abstract: Two-mm thick A1050 pure aluminum plates were successfully joined by conventional and rapid cooling friction stir welding (FSW), respectively. The microstructure and mechanical properties of the welded joints were investigated by electron backscatter diffraction characterization, Vickers hardness measurements, and tensile testing. The results showed that liquid CO_2 coolant significantly reduced the peak temperature and increased the cooling rate, so the rapidly cooled FSW joint exhibited fine grains with a large number of dislocations. The grain refinement mechanism of the FSW A1050 pure aluminum joint was primarily attributed to the combined effects of continuous dynamic recrystallization, grain subdivision, and geometric dynamic recrystallization. Compared with conventional FSW, the yield strength, ultimate tensile strength, and fracture elongation of rapidly cooled FSW joint were significantly enhanced, and the welding efficiency was increased from 80% to 93%. The enhanced mechanical properties and improved synergy of strength and ductility were obtained due to the increased dislocation density and remarkable grain refinement. The wear of the tool can produce several WC particles retained in the joint, and the contribution of second phase strengthening to the enhanced strength should not be ignored.

Key words: aluminum alloy; friction stir welding; recrystallization; microstructure; mechanical properties

1 Introduction

Friction stir welding (FSW) is a solid-state joining technology that was invented by The Welding Institute of U.K. in 1991[1]. FSW completely avoids the defects related to fusion welding methods, such as porosities and cracks, and thus provides a new approach in generating high-quality welded joints of aluminum alloys. Until now, scholars around the world have carried out extensive studies on FSW of aluminum alloys, including microstructural evolution[2], temperature distribution and material flow[3,4], and improvement of mechanical properties and corrosion resistance[5,6]. However, there are few reports on FSW of pure aluminum. Sato *et al*[7] conducted FSW on 1-mm thick A1050 pure aluminum, and it was found that the grain size of the welded joint was refined to less than 1 μm by decreasing the heat input. Compared with the base material (BM), the grain size of the welded joint was significantly refined, but the mechanical properties of the welded joint were remarkably lower than that of the BM, leading to unsatisfactory welding efficiency.

For metals or alloys, their mechanical properties can be further improved by simultaneously refining the grain size and increasing the dislocation density. In recent years, rapid cooling FSW (RCFSW) technology has been further developed to improve the microstructure and mechanical properties of the joints. During the RCFSW, a cooling device is used to limit the grain growth and increase the dislocation density of the joints, so the welding efficiency is significantly improved. High-pressure air gas, water, liquid CO_2, and liquid N_2 are often selected as coolants[8]. Zhang *et al* studied the microstructure and mechanical properties of RCFSW stainless steel joint associated with water cooing. They found that both the peak temperature and high temperature duration of the joint were significantly reduced. The joint exhibited an ultrafine stir zone (SZ) with its mean grain size of 900 nm and a heat affected zone with high dislocation density, resulting in a remarkably improved mechanical properties compared with those of conventional FSW joint[9]. Kumar *et al* conducted RCFSW with water cooling on the dissimilar 5083-6061 aluminum alloys. It was found

© Wuhan University of Technology and Springer-Verlag GmbH Germany, Part of Springer Nature 2024

(Received: Jan. 21, 2023; Accepted: Sept. 18, 2023)

XU Nan (许楠): Prof.; Ph D; E-mail: xunan20032389@126.com

Funded by the Natural Science Foundation of Jiangsu Province (No.BK20211067) and "Qing Lan" Project of Jiangsu Province

that the joint showed refined grain structure, highly enhanced dislocation density, and fine intermetallic compounds. Therefore, the joint exhibited the highest tensile strength and strain hardening capacity. In our previous study, RCFSW associated with liquid CO_2 coolant (–78 ℃) was conducted on 2-mm thick T2 pure copper[10]. An ultrafine-grained microstructure with high dislocation density formed in the welded joint and the mechanical properties were significantly improved. More recently, RCFSW technology associated with liquid N_2 coolant (–196 ℃) was performed on TA2 pure titanium. The processing temperature was strictly controlled below the α/β phase transformation temperature, and it was found that an ultrafine-grained microstructure with massive dislocations and {10-12} twins was generated in the welded joint, resulting in improved strength and ductility of the welded joint[11]. According to our previous studies, the use of strong coolant during FSW not only reduces the peak temperature but also increases the cooling rate. Pure copper and pure titanium have relatively low stacking fault energies of 78 and 31 mJ/m^2, respectively[12,13]. The reduced peak temperature and enhanced cooling rate can effectively inhibit dislocation recovery. Therefore, some dislocations produced during plastic deformation can be retained in the interior of the grain. Furthermore, grain coarsening was also inhibited. An ultrafine grain structure with abundant substructures formed, thus improving the mechanical properties of the welded joints. However, pure aluminum has a relatively high stacking fault energy of 166 mJ/m^2[14], and dynamic recovery easily occurs during high temperature plastic deformation. It is unclear whether RCFSW technology can produce an ultrafine grain structure with high dislocation density in the pure aluminum joints. Therefore, in this work, RCFSW associated with liquid CO_2 coolant was performed on 2-mm thick A1050 pure aluminum plates, and the microstructure evolution and mechanical properties were carefully investigated.

2 Experimental

Cold-rolled commercially A1050-H24 pure aluminum plates with dimensions of 200 mm × 100 mm × 2 mm were used in this work. The welding tool was made of WC-Co-based steel and equipped with a columnar probe with no thread. Before welding, the butt surface of the plates was ground with SiC sandpaper and then cleaned using acetone. The welding direction was parallel to the plate rolling direction. The liquid CO_2 cooling device was set 50 mm behind the welding tool and operated at the same speed as the welder. The schematic of the RCFSW process and welding tool are shown in Fig.1. For comparison, conventional FSW with air cooling was also conducted. The welding speed and tool rotation rate were set as 300 mm/min and 800 rpm, respectively. The plate normal direction, transverse direction, and welding direction are abbreviated as ND, TD, and WD, respectively.

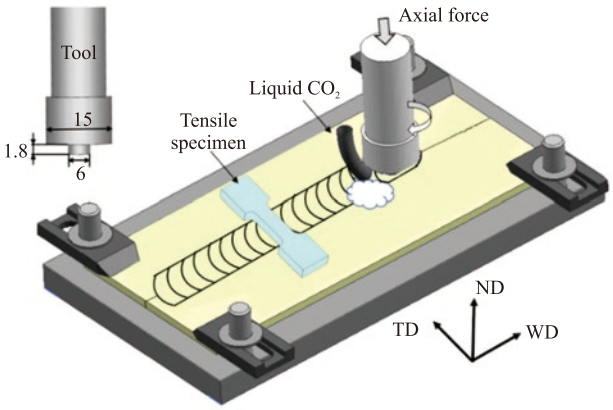

Fig.1 Schematic of the RCFSW process and welding tool

After the FSW, the cross-sectional specimens were cut perpendicular to WD, and then electro-polished with a mixture solution of 700 mL methanol, 100 mL perchloric acid, 100 mL ethanol, and 100 mL distilled water at a voltage of 20 V for 30 s. An electron backscattered diffraction (EBSD) camera attached to a field-emission gun scanning electron microscope (FEG-SEM) was used for microstructural characterization. EBSD measurements were conducted at the central SZ using a TSL OIM™ system, and the step size of each scanning was 0.2 μm. The Vickers hardness distributions of the welded joints were measured along the mid-thickness of the plates with a 50 g load for 15 s. The transverse tensile specimens covering various regions with a gauge size of 30 mm × 5 mm × 1.5 mm were machined with the tensile axis perpendicular to the WD. The tensile tests were carried out using an Instron-type testing machine with a crosshead speed of 1 mm/min.

3 Results and discussion

3.1 Microstructure evolution

EBSD characterization results of the SZs of FSW A1050 pure aluminum joints are shown in Figs.2-4. The conventional FSW and RCFSW joints exhibited uniform equiaxed grain structures with

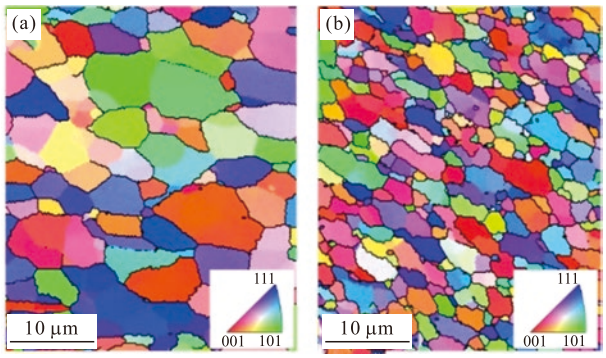

Fig.2 Inverse pole figure of the SZ of FSW A1050 pure aluminum joint: (a) Conventional FSW; (b) RCFSW

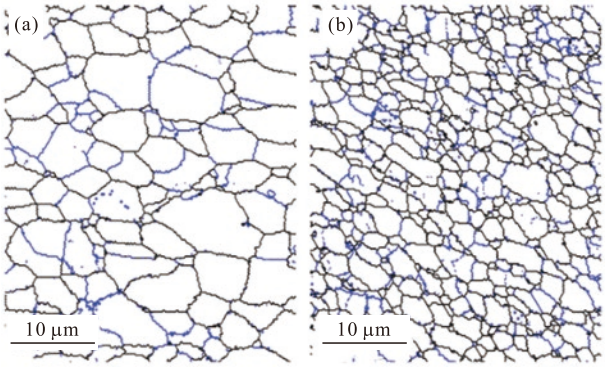

Fig.3 Grain boundary map of the SZ of FSW A1050 pure aluminum joint: (a) Conventional FSW;(b) RCFSW (The LAB and HAB (high angle boundary, $\theta \geqslant 15°$) are represented by blue and black, respectively)

average grain sizes of 5.3 and 2.6 μm, respectively (Fig.2). The number fraction of low angle boundary (LAB, $2° \leqslant \theta < 15°$) of conventional FSW and RCFSW was 25% and 29%, respectively (Fig.3 and Fig.4). It is known that LAB mainly consists of a dislocation structure[15]. It was indicated that although the same welding parameters were adopted, the grain size of the RCFSW joint was finer than that of the conventional FSW. Furthermore, the dislocation density in the RCFSW joint was higher than that of conventional FSW. Liquid CO_2 cooling effectively eliminated the post-annealing effect, and some dislocations produced during plastic deformation could be retained in the grain interiors. Moreover, the reduced migration speed of the grain boundaries inhibited the grain growth. Fig.5 shows the kernel average misorientation (KAM) of the SZs of conventional FSW and RCFSW joints. The higher KAM value indicates the higher dislocation density[16]. It can be seen that the KAM value of the RCFSW joint was higher than that of the conventional FSW joint, indicating that the SZ of the RCFSW joint had a relatively higher dislocation density. Therefore, compared with the conventional FSW joint, the RCFSW joint exhibited a refined grain structure with relatively high dislocation density.

The FSW joint usually exhibits shear texture due to the high-speed rotating probe. The shear texture is usually expressed in term of {*hkl*}<*uvw*>, *i e*, the close packed plane normal <*hkl*> and close packed direction <*uvw*> parallel to the shear plane normal (SPN) and shear direction (SD), respectively[17]. The typical shear textures and their Euler angles of face-centered cubic metals are shown in Fig. 6. To investigate the influence of welding thermal cycle on grain orientation, the textural features of the SZ were analyzed. Fig.7 shows the (111) and (011) pole figures of central SZs of FSW A1050 pure aluminum joints. Compared with the exact pole figures as shown in Fig.6, it was found that the original pole figures remarkably deviated from the standard pole figures. Due to the varying diameter between shoulder and probe, the shear plane was similar to a conical surface, resulting in SPN and SD changing with respect to material position. Therefore, to analyze the grain orientation of central SZ, the original pole figures should be rotated to ensure that the SPN and SD are parallel to the ND and TD, respectively[18]. Fig.8 shows the rotated (111) and (011) pole figures of the central SZs of the FSW A1050 pure aluminum joint. It can be seen that the central SZ of conventional FSW has a B/ type {112}<110> component with a maximum intensity of 6.5. The central SZ of the RCFSW joint mainly consists of two

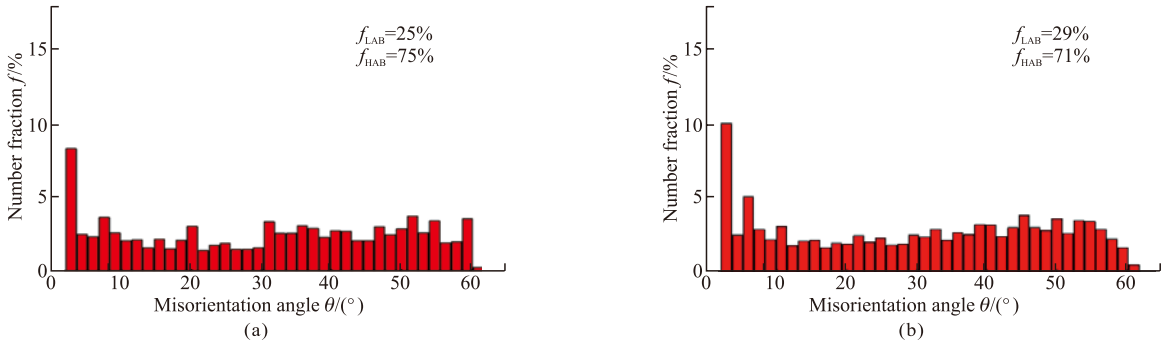

Fig.4 Histogram of the misorientation angle distribution of the SZ of FSW A1050 pure aluminum joint: (a) Conventional FSW; (b) RCFSW

components, *i e*, B/ type {112}<110> component and C type {001}<110> component, and the texture intensity was reduced to 4.9. Liu *et al* conducted conventional FSW and RCFSW on 3-mm thick A1050-H24 plates[21]. The results suggested that due to the high stacking fault energy of pure aluminum and severe plastic deformation, the grain refinement of the SZ was mainly attributed to continuous dynamic recrystallization. For the FSW of aluminum alloys, a mixture texture including the {112}<110> component and {001}<110> component usually formed in the SZ. Since the cooling rate of CFSW was relatively low, the recrystallized grains with a {112}<110> orientation grew fast due to the post-annealing effect, leading to the disappearance of the {001}<110> component.

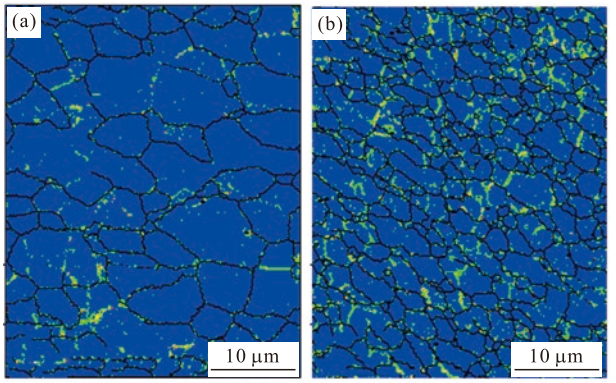

Min	Max	Total fraction	Partition fraction	Min	Max	Total fractior
0	1	0.940	0.940	0	0.989 408	0.852
1	2	0.049	0.049	0.989 408	1.978 82	0.132
2	3	0.005	0.005	1.978 82	2.968 23	0.012
3	4	0.001	0.001	2.968 23	3.957 63	0.003
4	5	0.001	0.001	3.957 63	4.947 04	0.001

Fig.5 KAM map of the SZ of FSW A1050 pure aluminum joint: (a) Conventional FSW;(b) RCFSW

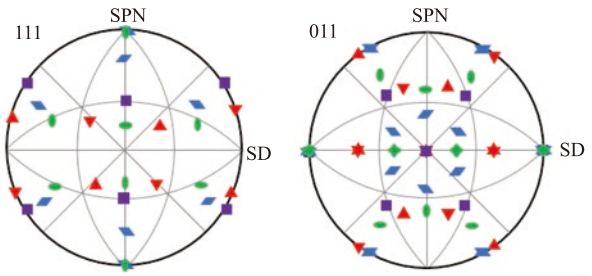

Texture	Description	Euler angles/(°)		
		φ_1	Φ	φ_2
A_1^*	{111}<$\bar{1}1\bar{2}$>	35.3/215.3	45	0
		125.3/305.3	90	45
A_2^*	{111}<$11\bar{2}$>	144.7/324.7	45	0
		54.7/234.7	90	45
A	{1$\bar{1}$1}<110>	0	35.3	45
$\bar{A}$	{1$\bar{1}$1}<$\bar{1}\bar{1}$0>	180	35.3	45
B	{1$\bar{1}$2}<110>	0/120/240	54.7	45
$\bar{B}$	{$\bar{1}$1$\bar{2}$}<$\bar{1}\bar{1}$0>	60/180/300	54.7	45
C	{001}<110>	90/270	45	0

Fig.6 Exact (111) and (011) pole figures and Euler angles of typical shear textures of face-centered cubic metals[20]

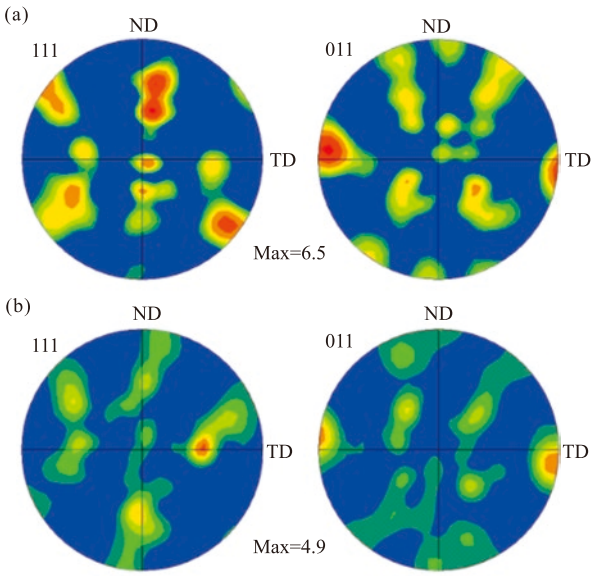

Fig.7 Original (111) and (011) pole figures of the SZs of FSW A1050 pure aluminum joints: (a) Conventional FSW; (b) RCFSW

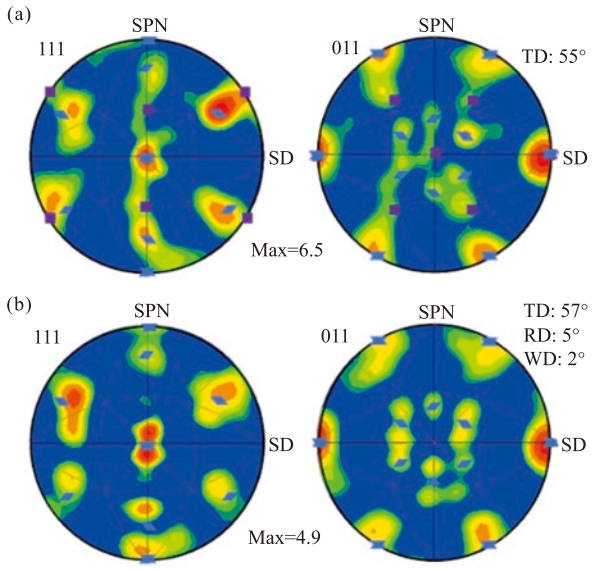

Fig.8 Rotated (111) and (011) pole figures of the SZs of FSW A1050 pure aluminum joints: (a) Conventional FSW; (b) RCFSW

Compared with the SZ, the peak temperature, strain, and strain rate of the thermo-mechanically affected zone (TMAZ) are relatively low, thus the TMAZ showed a partially recrystallized grain structure. Because the TMAZ is a transitional zone showing how the original structure transformed into a fine structure, the investigation of TMAZ can help us understand the grain refinement mechanism during the FSW of A1050 pure aluminum. Furthermore, due to the cooling effect of liquid CO_2, the dislocation recovery and grain growth were remarkably restricted. EBSD was conducted on the TMAZ of the RCFSW joint to study the grain refinement mechanism of FSW A1050 pure

aluminum. Fig. 9 shows the EBSD characterization results of the TMAZ of the RCFSW A1050 pure aluminum joint. It can be seen that TMAZ consisted of original coarse grains and fine recrystallized grains (Fig.9(a)). Previous studies suggested that the dominant grain refinement mechanism during the FSW of the aluminum alloy was continuous dynamic recrystallization[19]. In this work, the microstructural feature of continuous dynamic recrystallization was also identified, as indicated by the Arrow 1 in Fig.9(b). Initially, the plastic deformation caused increased dislocation density. Then, dislocation cells and LABs formed due to the continuous dislocation climb. When the misorientation of the grain boundary exceeded 15°, newly recrystallized grains surrounded by HAB were generated. Fig.10 shows the point-to-point misorientation distribution from the initial grain boundary to grain interior (Point A in Fig.9(a)). It was found that the misorientation gradually increased from the boundaries to grain interior, indicating that LAB formed initially at the original boundary during plastic deformation. Therefore, the new grains caused by continuous dynamic recrystallization preferentially appeared at the grain boundaries and then gradually propagated into the grain interior. Furthermore, due to the adoption of liquid CO_2 cooling, grain subdivision and geometric dynamic recrystallization were also identified. These two grain refinement mechanisms have not been reported in the FSW of A1050 pure aluminum. As shown by Arrow 2 in Fig.9(b), some new grains without substructures were found in the interior of the original grains. It was deduced that they formed via the grain subdivision mechanism[22,23]. At the initial stage of FSW, several micro shear bands formed in the original grains. Micro shear bands in different directions can adjust the stress concentration and cause the plastic deformation to become more coordinated. Sub-grains surrounded by LAB are preferentially formed at the intersection of micro shear bands. Due to the sub-grains being continuously absorbed in the dislocations, the misorientation of LAB gradually increased and finally changed into HAB. The volume fraction of new grains gradually increased until the original coarse grains were almost completely replaced, resulting in the formation of fine equiaxed grains. As shown by Arrow 3 in Fig.9(b), due to the combined influence of axial force and shear force introduced by the shoulder and probe, respectively, the original grains were elongated, and the initial straight grain boundary changed into a serrated shape. This is a typical

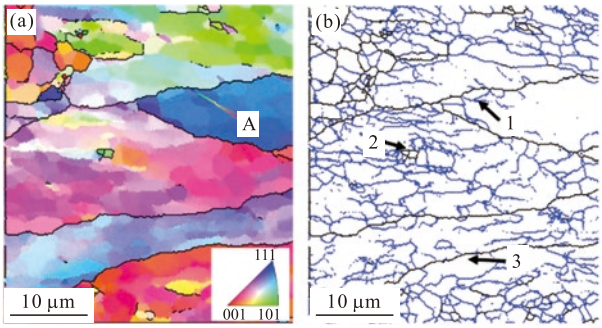

Fig.9 TMAZ of the RCFSW A1050 pure aluminum joint: (a) Inverse pole figure; (b) Grain boundary map

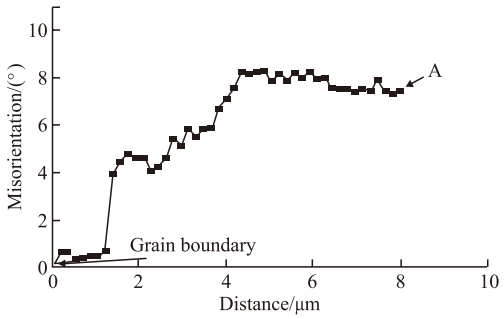

Fig.10 Point-to-point misorientation distribution along the grain boundary to Point A in Fig. 9(a)

characteristic of geometric dynamic recrystallization[24]. As the plastic deformation continuously proceeded, the original grains were further elongated and the spacing between grain boundaries narrowed. Subsequently, the serrations of the grain boundaries were pinned with each other, and fine equiaxed recrystallized grains formed. Grains formed by geometric dynamic recrystallization usually contain 2-3 sub-grains. In fact, whether processed via conventional FSW or RCFSW, the grain refinement of the welded joint is determined by the combined effects of continuous dynamic recrystallization, grain subdivision, and geometric dynamic recrystallization. For conventional FSW, due to the post-annealing effect, the substructures produced in the process of grain subdivision and geometric dynamic recrystallization disappeared, and the grains gradually grew and finally formed an equiaxed shape. The morphology of recrystallized grains originating from grain subdivision and geometric dynamic recrystallization is very similar to that of continuous dynamic recrystallization. Therefore, grain subdivision and geometric dynamic recrystallization are difficult to detect. For RCFSW, the cooling effect of liquid CO_2 can inhibit grain growth and dislocation recovery, and some substructures generated in the process of plastic deformation remained in the grains, which help to more accurately and comprehensively analyze the grain

refinement mechanism of FSW A1050 pure aluminum. To make it easier for readers to understand the grain refinement mechanism of pure aluminum during FSW, a schematic diagram is shown in Fig.11.

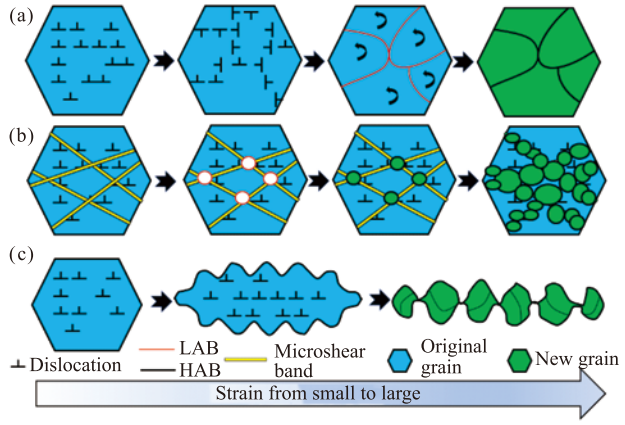

Fig.11 Schematic of the grain refinement mechanism of the FSW A1050 pure aluminum joint: (a) Continuous dynamic recrystallization; (b) Grain subdivision; (c) Geometric dynamic recrystallization

3.2 Mechanical properties

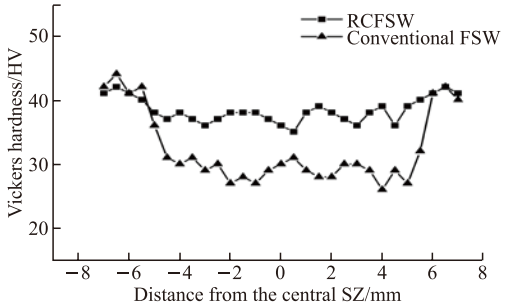

Fig.12 Vickers hardness distribution of FSW A1050 pure aluminum joints

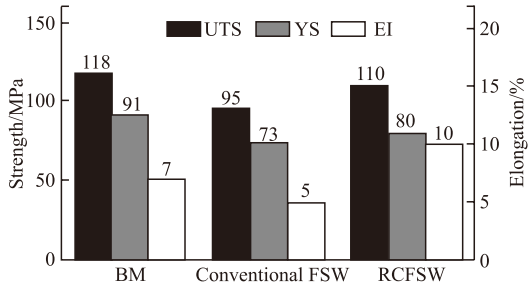

Fig.13 Tensile properties of as-received BM and FSW A1050 pure aluminum joints

Fig.12 shows the Vickers hardness distribution of the FSW A1050 pure aluminum joints. The average hardness of the joint after conventional FSW and RCFSW was 31 and 38 HV, respectively. Due to the effect of liquid CO_2 cooling, the post-annealing effect was eliminated. Grain growth and dislocation recovery were limited. Based on the combined influence of grain boundary strengthening and dislocation strengthening, the hardness of RCFSW was higher than that of conventional FSW.

Fig.13 shows the tensile properties of as-received BM and FSW A1050 pure aluminum joints. All tensile specimens were fractured at the weld center. The ultimate tensile strengths of the conventional FSW joint and RCFSW joint were 95 and 110 MPa, respectively, indicating the welding efficiency increased from 80% to 93% when using liquid CO_2 cooling. More importantly, both the yield strength and elongation were significantly improved, indicating that improved microstructure played a key role in the enhanced strength and ductility. The yield strength (σ_y) is mainly attributed to grain boundary strengthening and dislocation strengthening,

$$\sigma_y = \sigma_0 + \sigma_{g\text{-}b} + \sigma_{dislocation} \quad (1)$$

where σ_0 is the lattice friction stress (5.5 MPa) and $\sigma_{g\text{-}b}$ and $\sigma_{dislocation}$ are contributions of grain boundary strengthening and dislocation strengthening, respectively[25]. The contribution of grain boundary strengthening to yield strength can be calculated based on the following formula[26],

$$\sigma_{g\text{-}b} = K_{Al}(d/f_{HAB})^{-1/2} \quad (2)$$

where K_{Al} is a constant (0.04 $MPam^{-1/2}$), f_{HAB} is the number fraction of HAB, and d is the average grain size. In addition, the contribution of dislocation strengthening to yield strength can be calculated using the following formula [27],

$$\sigma_{dislocation} = M\alpha Gb\sqrt{\rho_{dislocation}+\rho_0} \quad (3)$$

where M is the Taylor factor (M=3.06) [26], α is a constant (α=0.24), G is shear modulus (G=26 GPa), b is Burgers vector (b=0.286 nm), ρ_0 is the dislocation density of pure aluminum under annealing state (1.23×10^{13} m^{-2}), and $\rho_{dislocation}$ is the dislocation density of the FSW joint. $\rho_{dislocation}$ can be predicted as follows,

$$\rho_{dislocation} = \frac{3f_{LAB}\theta}{bd} \quad (4)$$

where f_{LAB} is the number fraction of LAB and θ is the average misorientation of LAB.

According to Eqs.(1)-(4), the yield strength of the welded joint can be predicted using the following formula,

$$\sigma_y = \sigma_0 + K_{Al}(d/f_{HAB})^{-1/2} + M\alpha Gb\sqrt{\frac{3f_{LAB}\theta}{bd} + \rho_0} \quad (5)$$

Based on Eq.(5), the yield strengths of the conventional FSW joint and RCFSW joint were calculated as 68 and 72 MPa, respectively. It was found that the calculated results were relatively lower than that of the experimental values. During the FSW, severe friction occurred between high-speed rotating probe and base metal, resulting in wear of the probe surface. Few WC particles dropped from probe were introduced into the weld, which could have caused second phase strengthening. Patel *et al* studied the microstructure and mechanical properties of the FSW A7075 alloy joint. It was found that the hardness and strength were enhanced by 35% and 52% respectively compared with those of the BM due to dispersed WC particles[28]. In this work, only grain boundary strengthening and dislocation strengthening are considered as the dominant strengthening mechanisms. The effect of the second phase strengthening caused by the wear of the tool should not be ignored.

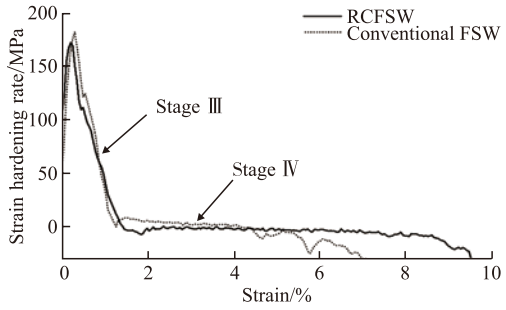

Fig.14 Strain hardening rate curves of FSW A1050 pure aluminum joints

Strain hardening rate is an important parameter describing the strain hardening behavior of materials[29]. Fig.14 shows the strain hardening curves of the FSW A1050 pure aluminum joint, which showed an initial sharp decrease and then a more gradual decrease. These two stages correspond to stage III and stage IV of the strain hardening behaviors for face-centered cubic metals or alloys. The RCFSW joint exhibited relatively small grain size and high dislocation density, so the proliferation rate of dislocations was larger than the annihilation rate during the tensile process. Therefore, the strain hardening rate of the RCFSW joint in stage III was higher than that of conventional FSW. As stretching proceeded, plastic deformation can be dispersed in more grains due to the remarkable grain refinement. The stress concentration was reduced, and the plastic deformation became uniform, so higher elongation was obtained.

4 Conclusions

In this work, thin commercial A1050 pure aluminum plates with 2-mm thick were subjected to conventional FSW and RCFSW. The microstructure and mechanical properties in the SZ were investigated, and the obtained conclusions are summarized as follows:

a) Liquid CO_2 cooling reduced the peak temperature and increased the cooling rate. The post-annealing effect was effectively eliminated, so the RCFSW joint exhibited a fine grain structure with high dislocation density.

b) The grain refinement mechanism of the FSW A1050 pure aluminum joint was attributed to the combined effects of continuous dynamic recrystallization, grain subdivision, and geometric dynamic recrystallization.

c) Compared with aluminum treated with conventional FSW, the yield strength, ultimate tensile strength, and fracture elongation of the sample treated with RCFSW were significantly improved, and the welding efficiency increased from 80% to 93%. The improved tensile behavior of the RCFSW joint was mainly attributed to grain refinement and enhanced dislocation density. The WC particles which caused by the wear of tool also contributes to the improvement of the strength.

Conflict of interest

All authors declare that there are no competing interests.

References

[1] Muangjunburee P, Naktewan J, Prachasaree W. Effect of Post-weld Heat Treatment on Microstructure and Mechanical Properties of Friction Stir Welded SSM7075 Aluminum Alloy[J]. *Journal of Wuhan University of Technology-Mater. Sci. Ed*., 2017, 32: 1 420-1 425

[2] Massardier V, Epicier T, Merle P. Correlation Between the Microstructural Evolution of A6061 Aluminum Alloy and The Evolution of Its Thermoelectric Power[J]. *Acta Mater.*, 2000, 48: 2 911-2 924

[3] Zhu Z, Wang M, Zhang H J, *et al*. Simulation on Temperature Field of Friction Stir Welding of 2A14 Aluminum Alloy Based on Equivalent Film Method[J]. *Key Eng. Mater.*, 2016, 723: 62-67

[4] Huang Y X, Wang Y B, Wan L, *et al*. Material-flow Behavior During Friction-stir Welding of 6082-T6 Aluminum Alloy[J]. *Int. J. Adv. Manuf. Technol*., 2016, 87: 1 115-1 123

[5] Huang Y X, Meng X C, Lv Z L, *et al.* Microstructures and Mechanical

Properties of Micro Friction Stir Welding (μFSW) of 6061-T4 Aluminum Alloy[J]. *J. Mater. Res. Technol*., 2019, 8: 1 084-1 091

[6] Sinhmar S, Dwivedi D K. Investigation of Mechanical and Corrosion Behavior of Friction Stir Weld Joint of Aluminum Alloy[J]. *Mater. Today: Proc.*, 2019, 18: 4 542-4 548

[7] Sato Y S, Urata M, Kokawa H, *et al*. Retention of Fine Grained Microstructure of Equal Channel Angular Pressed Aluminum Alloy 1050 by Friction Stir Welding[J]. *Scripta Mater.*, 2001, 45: 109-114

[8] Singh V P, Patel S K, Kuriachen B. Mechanical and Microstructural Properties Evolutions of Various Alloys Welded Through Cooling Assisted Friction-stir Welding: A Review[J]. *Intermetallics*, 2021, 133: 107 122

[9] Zhang H, Wang D, Xue P, *et al.* Achieving Ultra-high Strength Friction Stir Welded Joints of High Nitrogen Stainless Steel by Forced Water Cooling[J]. *J. Mater. Sci. Technol*., 2018, 34(11): 2 183-2 188

[10] Xu N, UEJI R, MORISADA Y, *et al.* Modification of Mechanical Properties of Friction Stir Welded Cu Joint by Additional Liquid CO_2 Cooling[J]. *Mater. Des*., 2014, 56: 20-25

[11] Xu N, Song Q N, Bao Y F, *et al.* Twinning-induced Mechanical Properties' Modification of CP-Ti by Friction Stir Welding Associated with Simultaneous Backward Cooling[J]. *Sci. Technol. Weld. Joining*, 2017, 22: 610-616

[12] CABALLERO V, VARMA S K. Effect of Stacking Fault Energy and Strain Rate on the Microstructural Evolution during Room Temperature Tensile Testing in Cu and Cu-Al Dilute Alloys[J]. *J. Mater. Sci*., 1999, 34: 461-468

[13] Guo Z, Miodownik A P, Saunders N, *et al.* Influence of Stacking-fault Energy on High Temperature Creep of Alpha Titanium Alloys[J]. *Scripta Mater*., 2006, 54: 2 175-2 178

[14] Liu X C, Sun Y F, Nagira T, *et al*. Effect of Stacking Fault Energy on the Grain Structure Evolution of FCC Metals during Friction Stir Welding[J]. *Acta Metall. Sin. (Engl. Lett.)*, 2020, 33: 1 001-1 012

[15] Tochigi E, Nakamura A, Shibata N, *et al.* Dislocation Structures in Low-Angle Grain Boundaries of α-Al_2O_3[J]. *Crystals*, 2018, 8: 133-147

[16] Xu N, Song Q N, Jiang Y F, *et al.* Large Load Friction Stir Welding of Mg–6Al–0.4Mn–2Ca Magnesium Alloy[J]. *Mater. Sci. Technol*., 2018, 34: 1 118-1 130

[17] Raturi M, Bhattacharya A. Microstructure and Texture Correlation of Secondary Heating Assisted Dissimilar Friction Stir Welds of Aluminum Alloys[J]. *Mater. Sci. Eng. A*, 2021, 825: 141 891

[18] Mironov S, Sato YS, Kokawa H. Microstructural Evolution During Friction Stir-Processing of Pure Iron[J]. *Acta Mater.*, 2008, 56: 2 602-2 614

[19] Liu X C, Sun Y F, Fujii H. Clarification of Microstructure Evolution of Aluminum During Friction Stir Welding Using Liquid CO_2 Rapid Cooling[J]. *Mater. Des.*, 2017, 129: 151-163

[20] Fonda R W, Knipling K E. Texture Development in Friction Stir Welds[J]. *Sci. Technol. Weld. Joining*, 2013, 16: 288-294

[21] Sakai T, Belyakov A, Kaibyshev R, *et al.* Dynamic and Post-dynamic Recrystallization under Hot, Cold and Severe Plastic Deformation Conditions[J]. *Prog. Mater. Sci.*, 2014, 60: 130-207

[22] Butler G C, Mcdowell D L. Polycrystal Constraint and Grain Subdivision[J]. *Int. J. Plasticity*, 1998, 14: 703-717

[23] Bay B, Hansen N, Hughes D A, *et al.* Evolution of FCC Deformation Structures in Polyslip[J]. *Acta Metal. Mater*., 1992, 40: 205-219

[24] Zhang J J, Yi Y P, Huang S Q, *et al.* Dynamic Recrystallization Mechanisms of 2195 Aluminum Alloy During Medium/High Temperature Compression Deformation[J]. *Mater. Sci. Eng. A*, 2021, 804: 140 650

[25] Huang T L, Shuai L F, Aneela W, *et al.* Strengthening Mechanisms and Hall-Petch Stress of Ultrafine Grained Al-0.3%Cu[J]. *Acta Mater*., 2018, 156: 369-378

[26] Wei Z, Shen Y, Zhang N, *et al.* Rapid Hardening Induced by Electric Pulse Annealing in Nanostructured Pure Aluminum[J]. *Scripta Mater*., 2012, 66: 147-150

[27] Kamikawa N, Huang X X, Tsuji N, *et al.* Strengthening Mechanisms in Nanostructured High-purity Aluminum Deformed to High Strain and Annealed[J]. *Acta Mater*., 2009, 57: 4 198-4 208

[28] Patel S K, Singh V P, Kumar D, *et al.* Microstructural, Mechanical and Wear Behavior of A7075 Surface Composite Reinforced with WC Nanoparticle Through Friction Stir Processing[J]. *Mater. Sci. Eng. B*, 2022, 276: 115 476

[29] Liu Q, Huang XX, Lloyd D J, *et al*. Microstructure and Strength of Commercial Purity Aluminum (AA 1200) Cold-rolled to Large Strains[J]. *Acta Mater.*, 2002, 50: 3 789-3 802